Actions of Cytochalasins on the Organization of Actin Filaments and Microtubules in a Neuronal Growth Cone

Paul Forscher and Stephen J Smith

Howard Hughes Medical Institute Research Laboratories, Yale University School of Medicine, Section of Molecular Neurobiology, New Haven, Connecticut 06510

Abstract. Actions of cytochalasin B (CB) on cytoskeletons and motility of growth cones from cultured *Aplysia* neurons were studied using a rapid flow perfusion chamber and digital video light microscopy. Living growth cones were observed using differential interference contrast optics and were also fixed at various time points to assay actin filament (F-actin) and microtubule distributions. Treatment with CB reversibly blocked motility and eliminated most of the phalloidin-stainable F-actin from the leading lamella. The loss of F-actin was nearly complete within 2–3 min of CB application and was largely reversed within 5–6 min of CB removal. The loss and recovery of F-actin were found to occur with a very distinctive spatial organization. Within 20–30 s of CB application, F-actin networks receded from the entire peripheral margin of the lamella forming a band devoid of F-actin. This band widened as F-actin receded at rates of 3–6 μm/min. Upon removal of CB, F-actin began to reappear within 20–30 s. The initial reappearance of F-actin took two forms: a coarse isotropic matrix of F-actin bundles throughout the lamella, and a denser matrix along the peripheral margin. The denser peripheral matrix then expanded in width, extending centrally to replace the coarse matrix at rates again between 3–6 μm/min. These results suggest that actin normally polymerizes at the leading edge and then flows rearward at a rate between 3–6 μm/min.

CB treatment was also observed to alter the distribution of microtubules, assayed by antitubulin antibody staining. Normally, microtubules are restricted to the neurite shaft and a central growth cone domain. Within ~5 min after CB application, however, microtubules began extending into the lamellar region, often reaching the peripheral margin. Upon removal of CB, the microtubules were restored to their former central localization. The timing of these microtubule redistributions is consistent with their being secondary to effects of CB on lamellar F-actin.

DURING neuronal development, growth cones guide growing neurites to their appropriate target site (24, 27). Growth cones are also the direct precursors to synaptic and neurosecretory terminals, undergoing dramatic structural changes upon target recognition; i.e., actin-based motility of lamellae ceases and specialized neurosecretory release sites are organized. Through this differentiation process, the growth cone is transformed into a relatively stable terminal capable of stimulus-evoked chemical signaling. What cytoskeletal rearrangements take place in the growth cone to transform this motile guidance system into a stable signaling device? We have examined the behavior of actin filaments and their interactions with microtubules in live neuronal growth cones as an experimental foundation for approaching this question.

Growth cones are spatially segregated into two distinct cytoplasmic domains, each characterized by a different form of motility. The central cytoplasmic domain, rich in organelles such as mitochondria and secretory granules, is characterized by directed organelle transport along microtubules. The peripheral (lamellar) cytoplasmic domain contains a dense actin network (28, 47) that excludes organelles. Growth cone lamellae in vitro exhibit two forms of motility: protrusive activity and ruffling. Lamellar ruffling is a characteristic feature of the leading edge of many motile cells (1, 14, 20, 39) and when observed in growth cones with time-lapse video recording, it takes the form of organized retrograde waves (17). These waves originate along the leading edge of the lamella and move centripetally at rates of 3–6 μm/min.

In a previous report we presented evidence that cAMP may be involved in regulation of growth cone structure (17). We found that elevation of cAMP inhibited the actin-based lamellar ruffling waves and resulted in extension of directed organelle transport into the formerly organelle-free lamellar region. These results suggested the possibility that peripheral actin networks might be an important factor in determining the spatial distribution of both organelle transport and microtubules.

In the present work, we have used cytochalasins to directly examine the consequences of disrupting actin networks on

growth cone structure and motility. Cytochalasins are well-characterized fungal metabolites that inhibit actin polymerization by capping the barbed end of actin filaments (7, 10, 13, 15, 18, 30, 31, 33), and that may also have other disruptive effects on actin filament networks (19, 35, 46). These agents are of physiological interest because they may act in a manner analogous to endogenous actin-capping proteins which have been the object of recent intense study (6, 11, 22, 25, 40).

Our observations of cytochalasin actions suggest that ongoing actin polymerization along the distal growth cone border is essential for protrusive activity and the generation of retrograde ruffling waves. In addition, cytochalasin treatments promoted microtubule extension accompanied by a distal spread of directed organelle transport. These findings suggest that actin filaments may also play an important role in determining the spatial distribution of microtubules and their associated transport functions.

Materials and Methods

Cell Culture

Laboratory reared *Aplysia californica* were provided by the Howard Hughes Medical Institute Marine Mariculture Facility at Woods Hole, MA. Dissociated bag cell neurons were plated on poly-D-lysine-coated coverslips in serum-free L-15 medium supplemented with seawater salts as previously described (17). Cells were then typically exposed to 0.5% FCS for 12–18 h before experimentation.

Video-Light Microscopy and Image Processing

An inverted microscope (model IM-35; Carl Zeiss, Inc., Thornwood, NY) set up for both differential interference contrast (DIC)[1] and fluorescence observation was used. The microscope was equipped with a 63×/1.4 NA Planapo objective, 1.4 NA oil immersion and 0.63 NA condensers, and fluorescence filter sets appropriate for selective observation of double labeling with rhodamine and fluorescein. Both Newvicon- and silicon-intensified target (SIT) tube type video cameras (model C2400; Hamamatsu Corp., Middlesex, NJ) were used to generate video signals which were processed with a digital image processor (Series 151; Imaging Technology Inc., Woburn, MA) controlled by an IBM PC-AT host computer. DIC images were processed to eliminate background mottle and shading by digitally subtracting an out-of-focus reference frame from the frame(s) of interest and sometimes by temporally averaging as well (2, 21). Low light level images of fluorescent probe distributions were obtained by integrating up to 256 video frames from the SIT camera. The SIT camera was used for both DIC and fluorescent probe observation when it was necessary to obtain a perfect correlation of structures observed in living growth cones with fluorescent labeling after fixation. This obviated the need to make difficult comparisons of images obtained from two different video cameras.

Image processing was accomplished using programs developed in this laboratory combined with commercially available function libraries and applications programs (Itex 151; Imaging Technology Inc. and Halo, Imagepro; Media Cybernetics, Silver Springs, MD). F-actin-microtubule composite images were made by digitally superimposing in two colors two different images generated from F-actin and microtubule fluorescence. Microtubule fluorescence image contrast was digitally enhanced by a single passage through a 3 × 3 pixel high pass convolution filter.

Experimental Treatments

Cells were mounted in double cover slip chambers (as previously described in reference 17) and constantly perfused at room temperature with artificial seawater (ASW) solution. ASW contained 400 mM NaCl, 10 mM KCl, 55 mM $MgCl_2$, 10 mM $CaCl_2$, 15 mM Na-Hepes, pH 7.6. After equilibration in ASW, cells were treated with cytochalasin B (CB) or cytochalasin D (Sigma Chemical Co., St. Louis, MO) and then fixed, permeabilized, and stained for the presence of F-actin and microtubules as described below. The fixation process was monitored by video microscopy at high magnification to enable optimization of fixation and permeabilization protocols for preservation of fine growth cone structure.

Fluorescent Labeling

The fixation buffer contained ASW with 4% formaldehyde and 400 mM sucrose added, pH 7.6. After fixation, cells were permeabilized for 2–5 min in fixation buffer plus 0.2% Triton-100, washed with PBS, and stained with rhodamine-phalloidin in PBS (Molecular Probes Inc., Eugene, OR). Cells were then washed with PBS, exposed to 10% normal goat serum-PBS followed by polyclonal rabbit antitubulin antibody (ICN Biochemicals, Inc., Lisle, IL), washed again with PBS, followed by 10% goat serum-PBS, exposed to FITC-conjugated goat anti-rabbit secondary antibody (Boehringer Mannheim Diagnostics, Inc., Indianapolis, IN), washed with PBS, transferred to a mounting solution (PBS supplemented with 20 mM *N*-propyl gallate [Sigma Chemical Co.] and 20% glycerol) and examined immediately for fluorescent staining. In control experiments where the tubulin primary antibody was omitted or cells were incubated with unlabeled phalloidin before exposure to fluorescent probes, there was little or no labeling observed.

Results

Normal Growth Cone Motility

Aplysia bag cell neuron growth cones display prominent and complex motility in their peripheral lamellar domains when observed using video-enhanced DIC time-lapse microscopy (17). One component of this motility takes the form of visible waves which originate along the distal margins of lamellae and move centripetally at rates of 3–6 μm/min. Because of their apparent direction of propagation, we refer to this form of lamellar motility as retrograde waves.

Fig. 1 illustrates examples of retrograde waves in growth cones under control conditions. A subarea was chosen for analysis in each growth cone (*black rectangle* in Fig. 1 *a*). Then a digital movie was made of each subarea using a 5-s interframe recording interval. The movie frames are displayed in a sequential video montage beneath the growth cone (Fig. 1 *b*). Retrograde waves appear as diagonal band patterns across the montage. Wave velocities can be calculated directly from the slope of the wave bands (4.0 μm/min for Fig. 1 *b*).

Under control conditions there is a clear demarcation between central and peripheral growth cone domains. Central domains are characterized by rapid directed transport of highly visible organelles, mainly 150–200-nm-diam neurosecretory granules and mitochondria (17). In contrast, peripheral domains (lamellae) have very low organelle density. The region of the growth cone comprising the central–peripheral interface where transported organelles meet retrograde waves will be referred to here as the transition zone (*arrowheads*, Fig. 1 *a*).

Bag cell growth cones plated in the absence of serum on poly-D-lysine substrates have a broad two-dimensional geometry with lamella ranging from 20–70 μm in width. This flat geometry is probably due to tight adherence to the poly-D-lysine substrate under serum-free plating conditions. High growth cone adhesivity was essential for this study because it prevented membrane detachment during prolonged CB exposures allowing careful analysis of drug-induced structural changes. Note that the growth cone extension rates we observe (4–10 μm/h) are somewhat slower than those typically observed in vertebrate growth cones (8–29 μm/h; reference

1. *Abbreviations used in this paper*: ASW, artificial seawater; CB, cytochalasin B; DIC, differential interference contrast; SIT, silicon-intensified target.

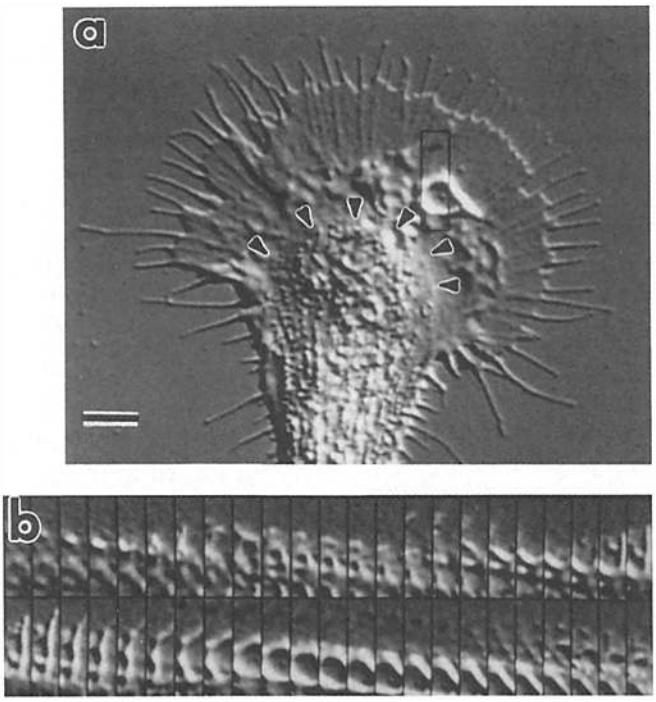

Figure 1. Retrograde wave motility in lamellae. (*a*) Video-enhanced DIC image of a growth cone indicating the subarea (*rectangle*; 2.7 × 10.2 μm) analyzed for retrograde wave activity. *Arrowheads*, the transition zone. (*b*) Video sequence of waves captured from the subarea in *a* at 5-s intervals. Wave velocity is proportional to the slope of the wave fronts (4.0 μm/min). Bar, 5 μm.

3). This may be due to nonspecific adhesive properties of poly-D-lysine, since *Aplysia* growth cones plated on a more physiological substrate (laminin) appear to have faster extension rates (unpublished observations).

Normal F-Actin and Microtubule Domains

To correlate the motility patterns described above with underlying cytoskeletal elements, growth cones were fixed, permeabilized, and then stained with fluorescent probes for F-actin and tubulin.

Fig. 2 shows a growth cone before (*a*) and after (*b*) fixation and permeabilization. F-actin structures visualized with rhodamine-phalloidin (4, 48, 49) are shown in Fig. 2 *c*; the microtubule distribution in the same field visualized by secondary immunofluorescence is shown in Fig. 2 *d*.

Under control conditions, F-actin labeling was concentrated in the peripheral growth cone domain (Figs. 2 *c* and 3). Patches of intense but diffuse phalloidin staining which probably correspond to areas of relatively random filament orientation were often observed in the transition zone (Fig. 2 *c*, *arrow*). Radial actin bundles aligned with filopodia project centrally from the lamellar border of motile growth cones. Alignment of actin bundles with filopodia can be seen most clearly in Fig. 3 *c* (*arrow*). These linear bundles have their proximal termination in the transition zone where they overlap with microtubule ends. Radial bundles appeared randomly bent for 2–5 μm in this region (Fig. 3, *a* and *b*, *arrows*). It may be noteworthy that the proximal border of intense F-actin staining coincides with the extreme boundary of observable organelle transport, suggesting that intact actin networks may play a role in determining organelle transport domains as will be considered below.

Arrays of aligned microtubules were always found in the central domain characterized by organelle transport (Fig. 2 *d*, asterisks mark leading edge of growth cone). In highly motile growth cones, most microtubules appeared to terminate in the transition zone mentioned above. Microtubule density fell off rapidly as the axial microtubule mass splayed out distally and individual microtubules or bundles could then be clearly resolved (Fig. 2 *d*, *arrowhead*). A few microtubules in a growth cone were usually observed to extend beyond the transition zone, sometimes extending to the distal growth cone margin. It should be stressed, however, that microtubule density observed in lamellae is extremely low relative to that observed in central domains. Also, although occasional microtubule ends extended into the transition zone, directed organelle transport was not observed beyond the proximal transition zone boundary.

To illustrate the differing spatial distributions of these two cytoskeletal elements, F-actin and microtubule images from both fluorescent probes were digitally superimposed (Fig. 9 *a*). Red codes for microtubules and blue for F-actin. Regions of overlap appear pink. Note that the tubulin antibody labels the axonal process running down the right side of the field (Fig. 9 *a*) which is essentially devoid of F-actin, and also that microtubules are restricted mainly to the central growth cone domain.

CB Effects on Growth Cone Motility

Figs. 4 and 5 illustrate the effects of CB on growth cone structure. In parallel with these structural effects, exposure to 0.1–10 μM CB resulted in rapid inhibition of lamellar retrograde waves and protrusive activity in lamellae and filopodia. CB effects on both structure and motility were totally reversible and occurred in a repeatable and highly stereotyped fashion. The effects reported here are representative of the effects of CB observed in >100 experiments.

Fig. 4, *a* and *b*, shows the growth cone immediately before and after 1 min in 5 μm CB. Concentrations of CB $\geq$ 2 μM resulted in apparent recession of lamellar actin networks. This usually occurred as a synchronous event along the entire distal growth cone margin within 1 min of CB exposure. The open arrows in Fig. 4 *b* point to the edge of the receding lamellar actin network after 1 min in CB (see also Fig. 5, *b* and *c*). Recession rates were 3.5 ± 0.5 μm/min (at $t \geq 90\%$) in 5–10 μM CB; note that these rates are similar to the propagation rates of retrograde waves described above. Recession rates were not significantly different between 5 and 10 μM CB. The presence or absence of retrograde movement observed in time-lapse video at a given point on the lamella was correlated with the presence or absence of actin networks at that point. After 5 min in CB, lamellar motility was always totally inhibited due to complete recession of peripheral actin networks into the central growth cone domain. Filopodial and lamellar protrusive activity and lateral filopodial movements were absent after 1–2 min exposure to CB and after 3–5 min in CB filopodia had usually retracted.

After 4–5 min in CB, directed organelle transport was observed to spread distally into the growth cone periphery. After 20–30 min in CB, organelles were often observed being

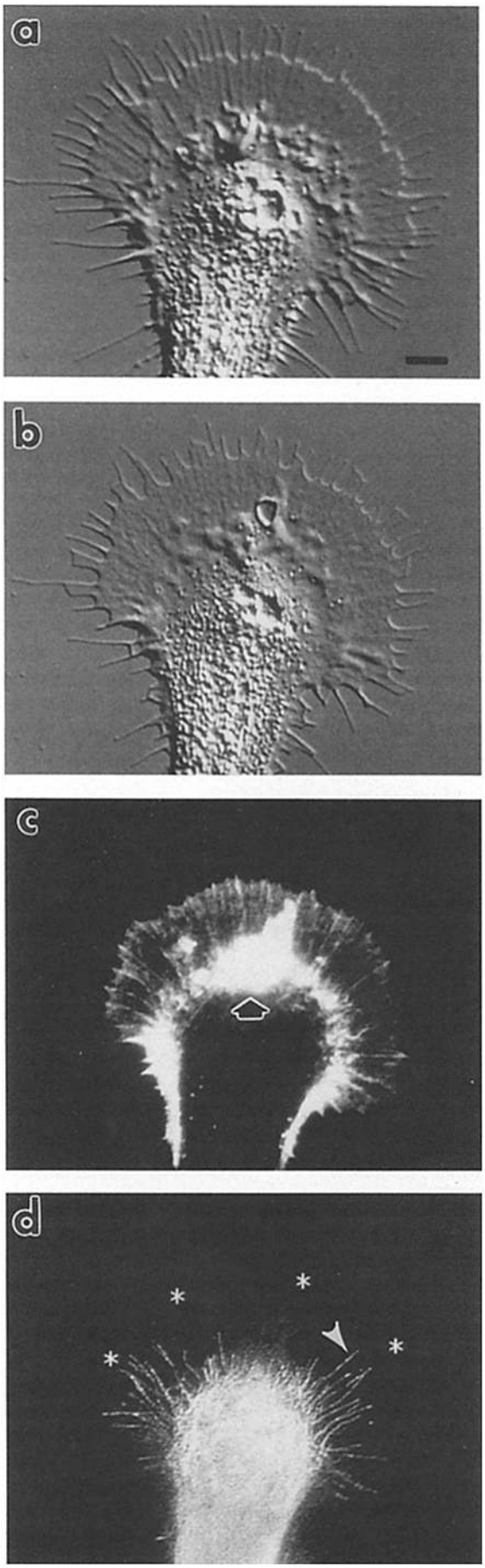

transported in both directions along clearly discernible linear elements to the distal margin of the growth cone (Fig. 4 *c*, *open arrows*). In these growth cones this amounts to extension of the central domain by 20–35 μm at a rate of ~1 μm/min.

In some cases, cytoplasmic elements which appeared to be microtubules were observed to extend at much more rapid rates (12–18 μm/min). These elements were capable of rapid translocation and formed hairpin loops that would coil and uncoil in a snakelike fashion in the growth cone periphery. A motile hairpin loop is illustrated in Fig. 4 *c* (*closed arrowhead*). Whether these loops represent individual microtubules or bundles, and whether extension results from polymerization or sliding has not been determined.

Removal of CB from the medium allowed rapid (5 min) and complete recovery of growth cone motility and structure as illustrated in Fig. 4 *d*. Details of the effects of CB on growth cone motility are discussed next.

Fig. 5, *a–e*, shows a growth cone at higher magnification under control conditions and after 0.5, 1, 3, and 9 min in 10 μm CB. Immediately after CB treatment, the distal edge of the receding lamellar cytoplasmic matrix is clearly observed (Fig. 5, *b* and *c*, *arrowheads*). After 3–9 min in CB lamellar motility was blocked and there is no evidence of organized structure in the peripheral regions of the growth cone (Fig. 5, *d* and *e*). Note that after 9 min of CB exposure (Fig. 5 *e*), all of the filopodia in this growth cone have retracted. The randomly dispersed granular accumulations in the lamella (Fig. 5 *e*, *arrows*) will be shown to be aggregates of short actin filaments (see Fig. 7 *e*). Directed organelle transport rates did not appear to be affected by CB treatments (2.5 and 2.6 μm/s before and after CB, respectively). The arrowhead in Fig. 5 *d* points to an isolated organelle that was undergoing directed transport.

After return to control solution, the first observable signs of recovery of lamellar actin structures were rapid formation of a coarse isotropic matrix in the growth cone periphery (Fig. 5 *f*, *large arrows*) accompanied by broadening and thickening of a dense actin matrix along the distal margin of the growth cone (Fig. 5 *f*, *small arrowheads*). Note that coarse matrix interfilament focci often occur in register with the punctate F-actin aggregates evident in Fig. 5 *e* (*arrows*). Both actin matrices appeared to translocate centripetally; however, a distinct change in the newly formed actin structures occurred during the initial recovery phase. Centripetal movement of actin resulted in disappearance or replacement of the coarse proximal matrix structure evident in Fig. 5 *f* (*large arrows*) with the denser matrix that appeared to be organized at the distal growth cone margin. A concentric boundary line which moved centripetally at 3–6 μm/min could be discerned between the coarse and dense actin matrices midway through the recovery process (Fig. 5 *g*, *open arrows*). Radially aligned actin bundles in register with newly formed

Figure 2. Normal F-actin and microtubule domains in growth cones. (*a*) Video DIC image of live growth cone just before fixation. (*b*) Same field as in *a* after fixation. (*c*) SIT camera image of F-actin distribution visualized with rhodamine-phalloidin. Note selective staining of peripheral growth cone domain and actin hot spot in the transition zone (*arrow*). (*d*) Microtubule distribution in same field. *Asterisks*, the growth cone border. Bar, 5 μm.

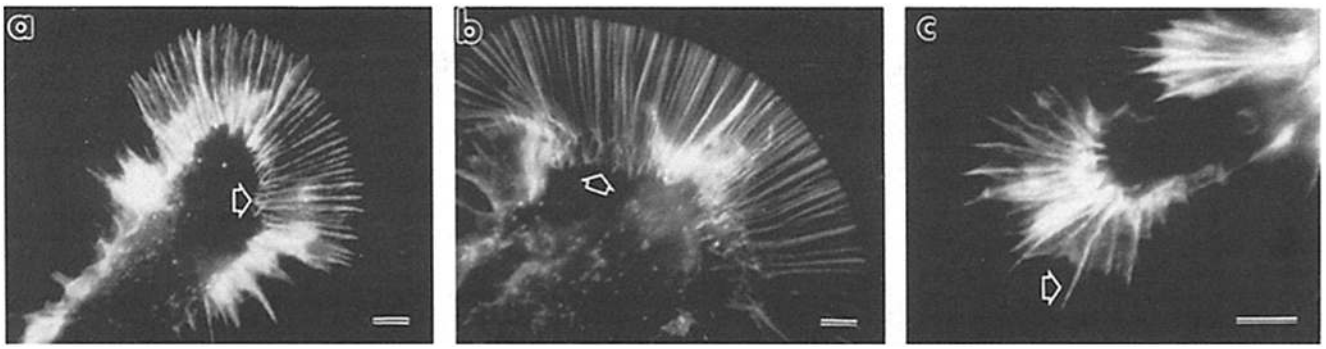

Figure 3. Normal F-actin patterns in motile growth cones. (*a–c*) Rhodamine-phalloidin fluorescence patterns in three growth cones. Note bending of radial actin bundles in the transition zones (*a* and *b*, *arrows*) and alignment of radial bundles with filopodia (*c*, *arrow*). Bars, 5 μm.

filopodia appeared only after disappearance of the coarse actin matrix (Fig. 5 *h*, *arrow*). Retrograde wave rates measured immediately after recovery (3.5 ± 1.2 μm/min, $t \geq 90\%$) were comparable to lamellar recession rates induced by CB and retrograde waves in untreated growth cones (3.5 ± 0.5 and 3–5 μm/min, respectively).

As a control for possible CB effects caused by alteration of hexose transport, experiments were performed using cytochalasin D (18, 31, 36). Results similar to those described above were obtained with cytochalasin D; however, recovery from cytochalasin D was a slower process. CB was chosen for use in this study because of its ready reversibility.

F-Actin and Microtubule Distributions After Brief CB Exposure

Growth cones were treated with CB and fixed after 1–2 min of drug exposure when cytoplasmic recession was clearly evident along the distal growth cone border. F-actin and

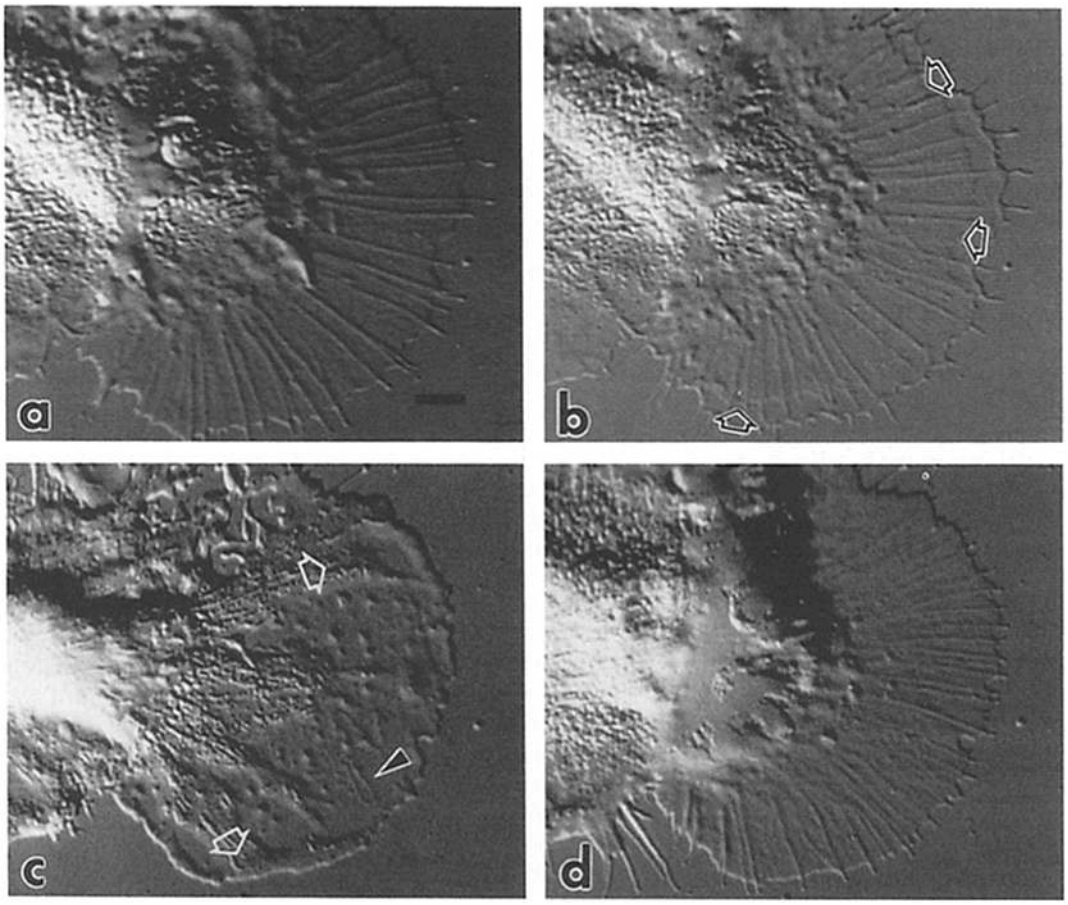

Figure 4. Effects of 5 μM CB treatment. (*a*) Control growth cone. (*b*) After 1-min CB exposure. Note the clear space between the edge of the receding cytoplasm (*open arrows*) and the distal growth cone margin. (*c*) After 30 min in CB-directed organelle transport extends to distal growth cone border (*open arrows*). *Arrowhead*, looped microtubule(s). (*d*) Recovery 20 min after CB washout. Bar, 5 μm.

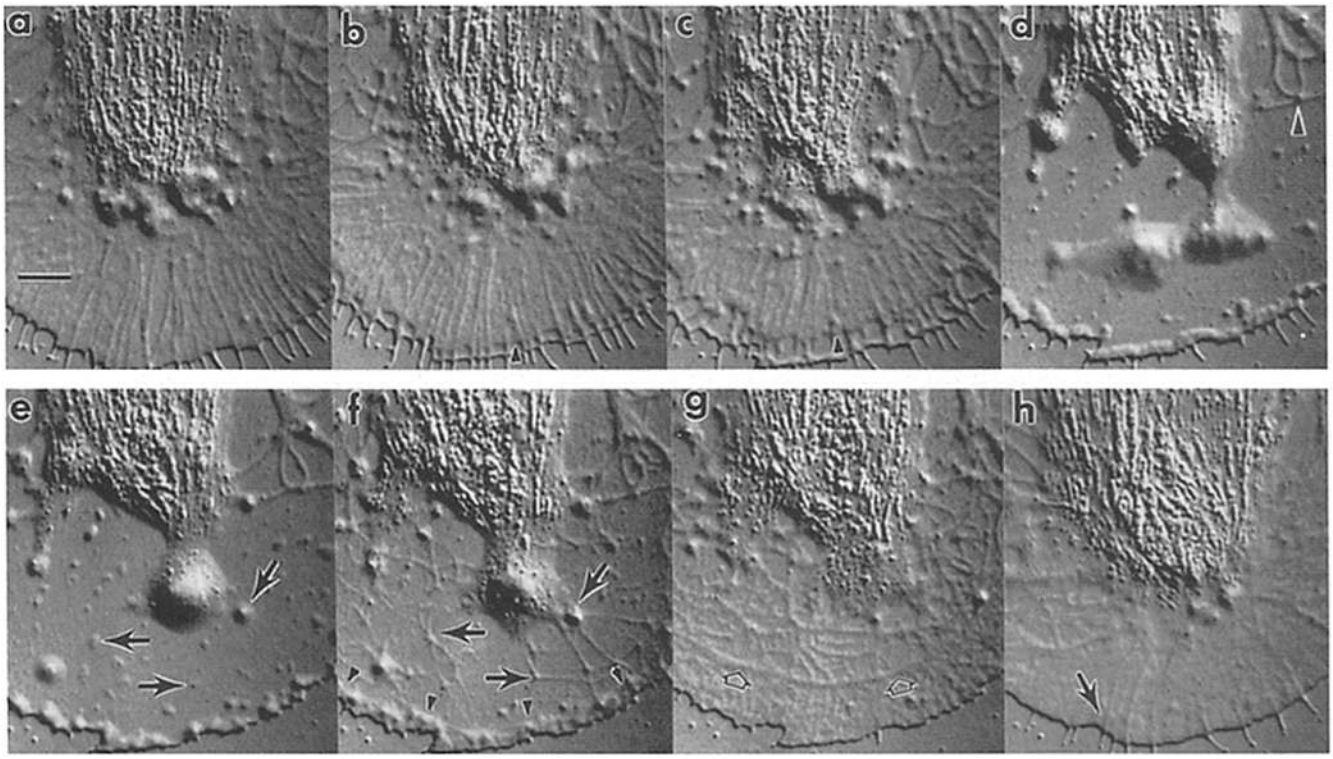

Figure 5. Effects of 10 μM CB seen at high magnification. (*a*) Control field. (*b–e*) After 0.5, 1, 3, and 9 min in CB. Note network recession along distal growth cone border (*b* and *c*, *arrowheads*) and microtubule bundles (*d*, *arrowhead*). (*f–h*) Recovery after 1-, 3-, and 17-min CB washout. Note that punctate actin aggregates in *e* (*arrows*), become interfilament foci in the isotropic actin webwork in *f* (*arrows*). Arrowheads in *f* point to thickening along the distal growth cone margin. Proximal boundary of the advancing retrograde wave front is marked in *g* (*arrows*). Growth cone has sprouted filopodia in register with radial actin bundles after 17 min of recovery in ASW (*h*, *arrow*). Bar, 5 μm.

microtubule distributions were then determined to investigate the structural changes in lamellar actin networks and microtubules underlying this characteristic early response to CB.

Fig. 6, *a* and *b*, shows a growth cone in ASW and after 80 s in 5 μM CB–ASW immediately before fixation. In Fig. 6 *b*, a gap has formed along the distal growth cone margin (*arrowheads*) due to recession of what appears to be essentially intact lamellar actin networks in this video DIC image. Rhodamine–phalloidin labeling of the same field (Fig. 6 *c*) verifies this interpretation of the DIC image revealing the presence of organized actin filament networks separated from the distal growth cone margin by a 6-μm gap. Note that apart from recession, actin network structure in briefly treated growth cones resemble controls and there is little or no evidence of random filament severing or disruption of radial actin organization in either Fig. 6, *e* or *c*. A distinct bead of F-actin labeling remains along the growth cone margin (Fig. 7, *c* and *e*). It will be shown below that a population of CB-resistant filaments are localized here as labeling in this region persists even after prolonged CB exposure.

Microtubule distributions did not differ appreciably from controls in growth cones fixed after brief CB exposures. Microtubule distribution for the same field is shown in Fig. 6 *d*; the growth cone border is indicated by asterisks. F-actin and microtubule distributions from another field from the same experiment are illustrated in Fig. 6, *e* and *f*. Similar results were obtained using a CB-dose range from 2 to 10 μM.

F-Actin and Microtubule Distributions After Prolonged CB Exposure

Treatment with 1–10 μM CB for ≥5 min resulted in distal extension of the region of directed organelle transport beyond the original transition zone. Experiments were done to test whether extension of microtubules accompanied this CB-induced extension of directed organelle transport.

Fig. 7, *a–d*, shows a growth cone before and after 1.5, 5, and 30 min in 10 μM CB. Exposure to CB for 30 min resulted in recession of the lamellar cytoplasm followed by distal advance of the organelle transport boundary at a net rate of ~1 μm/min. Microtubule immunofluorescence (Fig. 7 *f*) confirmed that the extended transport substrates were indeed microtubules. Note that individual elements where isolated organelle movements could be easily observed correlate well with microtubule labeling (Fig. 8, *d* and *f*, *arrowheads*, respectively).

F-actin networks and radial filament bundles were completely eliminated (Fig. 7 *e*) after prolonged CB exposures. Rhodamine–phalloidin labeling after prolonged CB was restricted to randomly dispersed aggregates of short filaments similar to those reported by others (26, 45), and a distinct bead of labeling along the distal growth cone margin. Chronic exposure to lower CB concentrations (≥1 μM) had similar

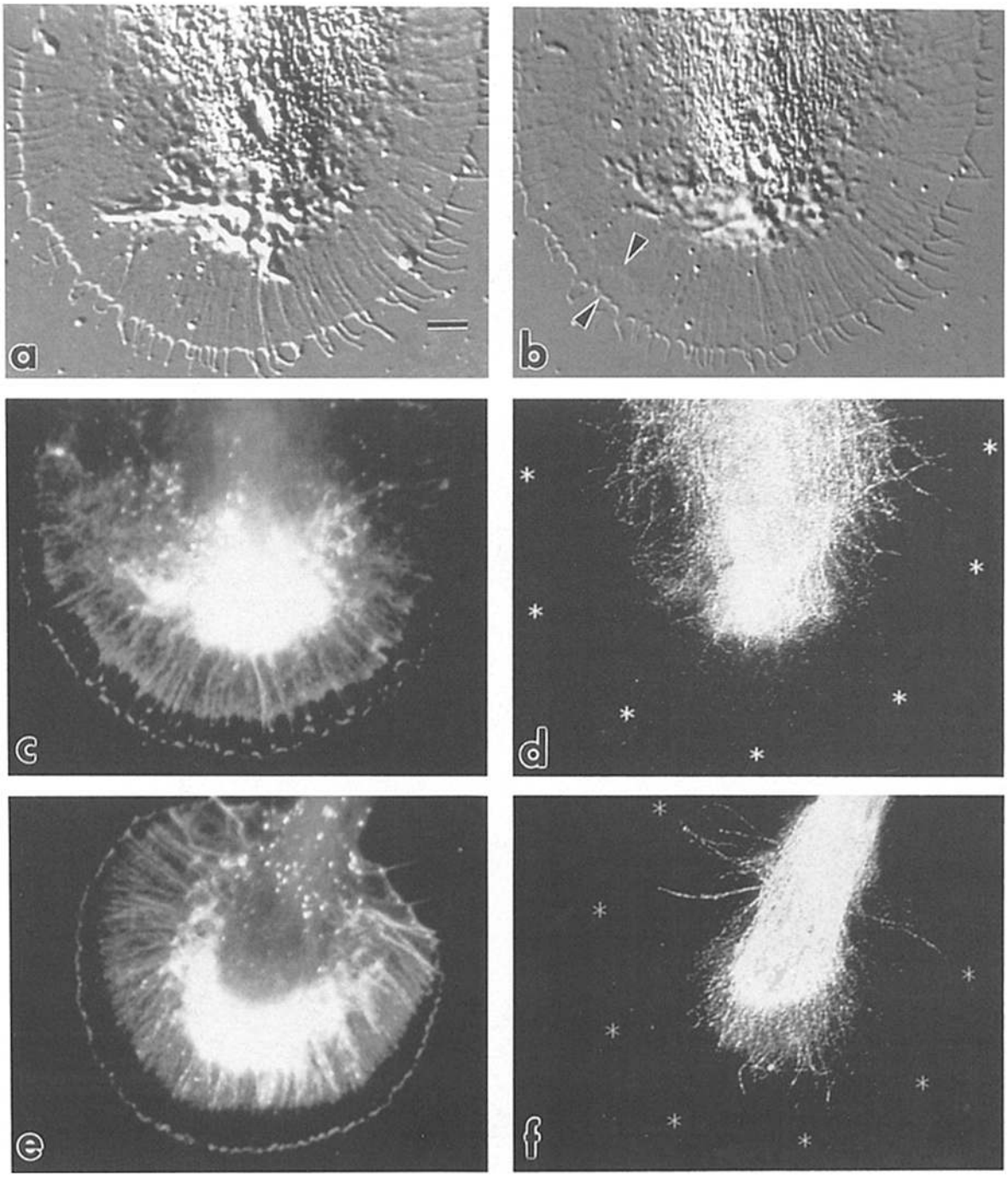

Figure 6. F-actin and microtubule domains after acute 5 μM treatment. (*a*) Control (*b*) After 80 s in CB. *Arrowheads*, gap along the distal growth cone margin. (*c* and *d*) F-actin and microtubules visualized in the same field as *b*. Note gap in actin network along distal growth cone border in *c*. Distal growth cone border is marked with asterisks in *d*. (*e* and *f*) Another F-actin–microtubule pair from the same experiment, also showing a clear recession of actin matrix along distal border. Microtubule distribution resembles controls at this early timepoint. Bar, 5 μm.

end effects on both F-actin and microtubule domains as higher CB doses.

Actin Polymerization During Recovery From CB

Examination of the initial phase of recovery from CB treatment (Fig. 5, *f* and *g*), suggested that actin was being reassembled into a dense matrix along the leading edge of the growth cone and also into a coarse isotropic matrix in more proximal regions. Fig. 8 illustrates a growth cone fixed and probed with rhodamine–phalloidin during recovery from CB when both of these matrices were clearly present. Fig. 8, *a–c*, shows the growth cone before CB treatment (Fig. 8 *a*), after 95 s in CB (Fig. 8 *b*), and immediately after return to control medium after a total of 155 s in CB (Fig. 8 *c*). The

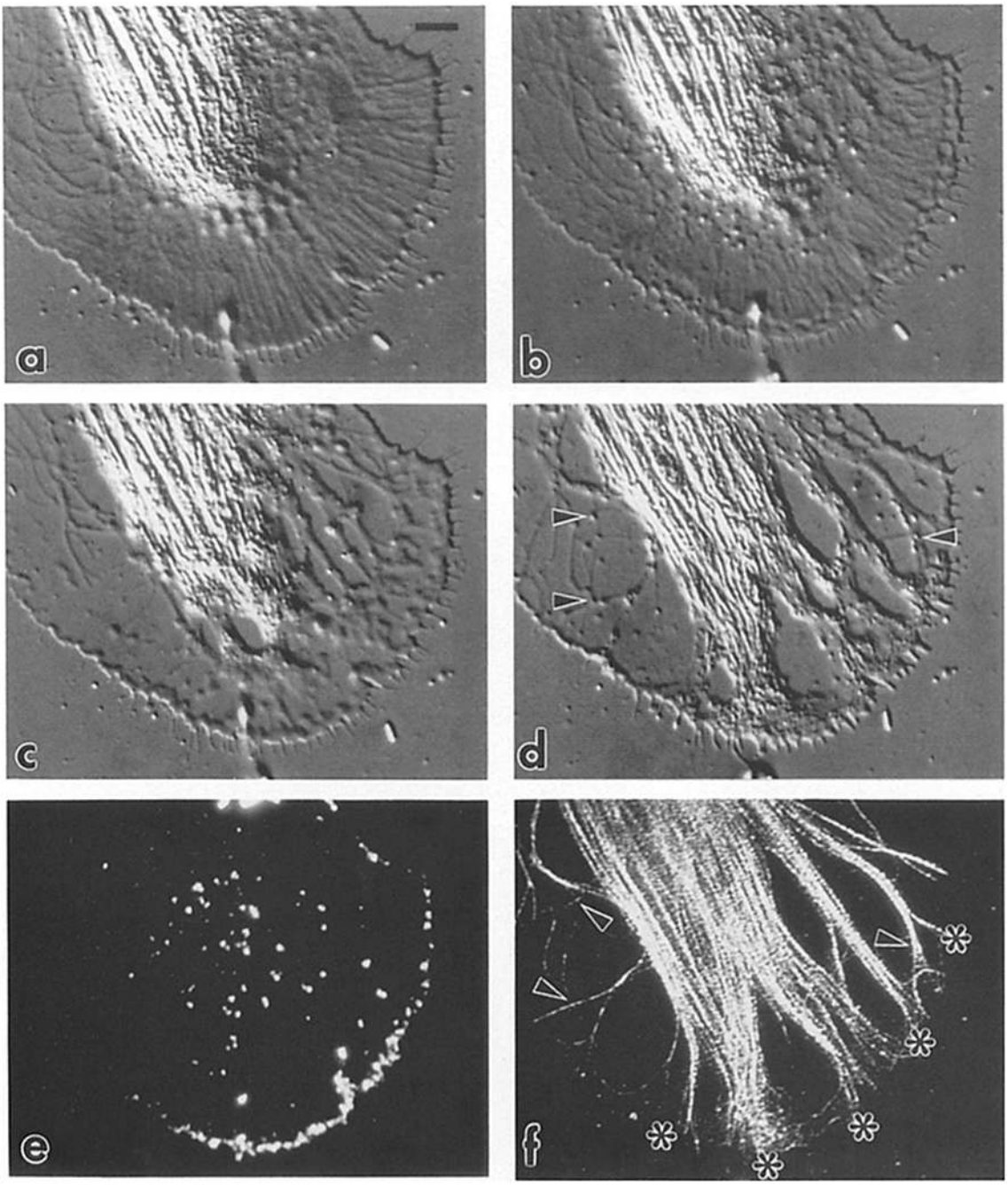

Figure 7. Microtubules extend as a result of CB treatment. (*a*) Control. (*b–d*) After 1, 5, and 30 min in 10 μM CB. *Arrowheads*, organelles being transported on microtubules in *d*. (*e* and *f*) F-actin and microtubule distributions, respectively, at 30-min timepoint. Actin networks are totally disrupted. *Asterisks*, growth cone border in *f*. Note correspondence between microtubules and organelle transport substrates (*arrowheads*). Bar, 5 μm.

arrow in Fig. 8 *b* points to the distal edge of receding F-actin. Note that lamellar actin networks were fully retracted when the growth cone was returned to control medium (Fig. 8 *c*). After 65 s of recovery, a dense matrix of actin along the peripheral growth cone margin began to form (Fig. 8 *d*, *arrowheads*) and the first signs of the coarse isotropic actin matrix discussed above were visible (Fig. 8 *d*, *open arrow*). 35 s later in the recovery, both matrices were clearly discernible (Fig. 8 *e*). At this time point the growth cone was fixed and probed for F-actin with rhodamine-phalloidin (Fig. 8 *f*). F-actin was concentrated in a band along the growth cone periphery that corresponds to the dense matrix described above (Fig. 8 *f*, *arrowheads*). The coarse matrix proximal to the dense recovery front is also labeled (Fig. 8 *f*, *open arrow*). The intensity of F-actin labeling in this region was always lower than that observed along the leading edge.

The density of F-actin labeling observed in the central cytoplasmic domains of growth cones was variable; labeling in this region in Fig. 8 *f* probably reflects the presence of less CB-sensitive actin networks that were not significantly dis-

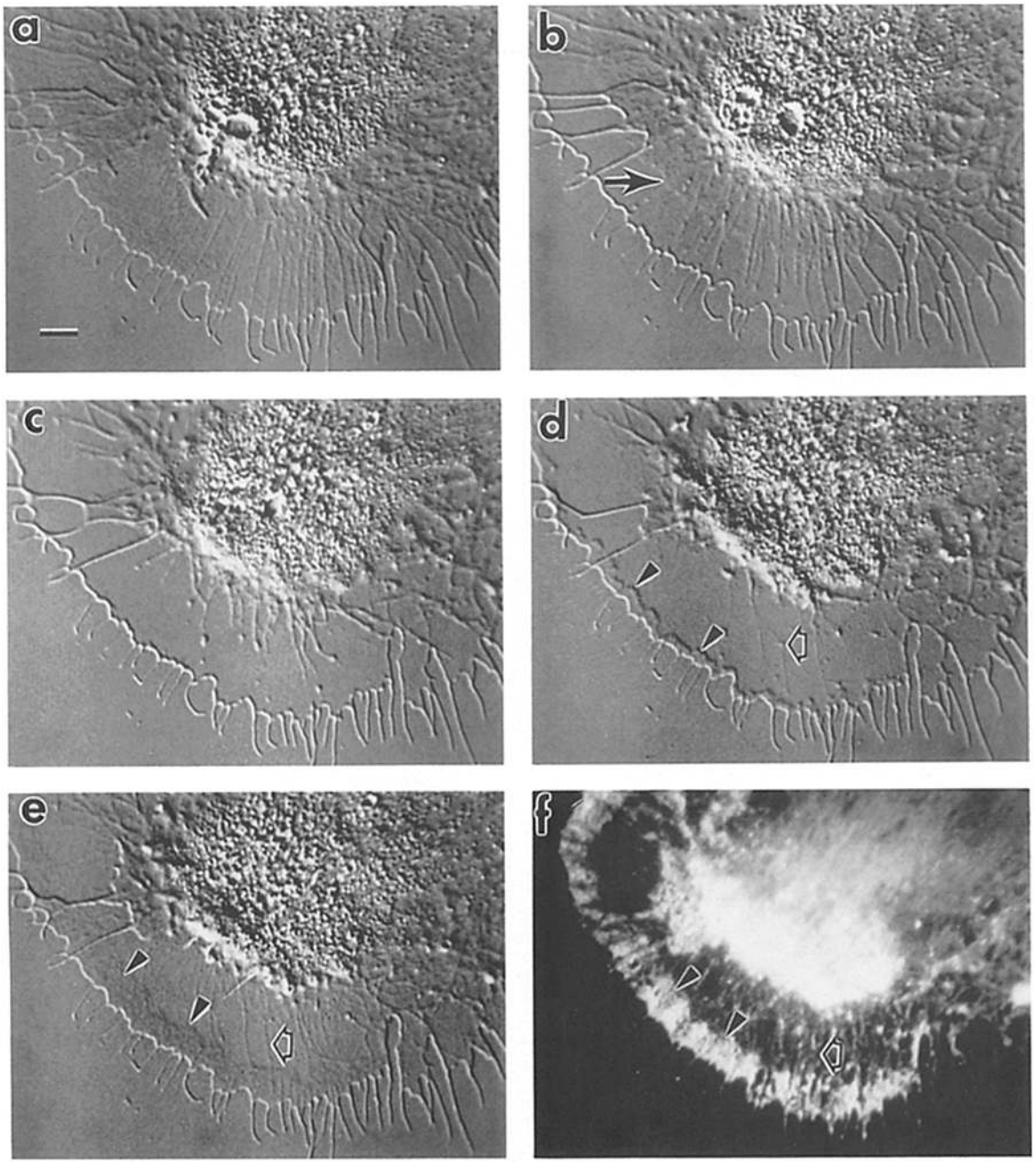

Figure 8. Actin polymerization and network assembly occurs preferentially at the leading edge. (*a*) Control. (*b*) After 95 s in 5 μM CB; *arrow*, distal edge of receding lamellar actin. (*c*) Immediately after return to control medium after a total of 155 s in CB, note complete absence of lamellar actin networks. (*d*) After 65-s recovery, the first signs of actin network assembly appear as a dense swelling along the growth cone margin (*arrowheads*) and proximal coarse matrix. *Open arrow*, an intersection in the coarse matrix. (*e*) After 100-s recovery both dense and coarse matrices (*arrowheads* and *open arrow*, respectively) are clearly observable. (*f*) Rhodamine-phalloidin labeling of F-actin for the same field as in *e*. *Arrowheads*, heavily labeled dense actin matrix; *open arrow*, elements of the coarse matrix. Bar, 5 μm.

rupted by the short (155 s) CB exposure. The hot spot in the transition zone in Fig. 8 *f* is also observed under control conditions (cf. Fig. 2 *c*) and in growth cones after relatively brief CB exposure (cf. Fig. 6, *c–e*), and is likely due to the presence of randomly oriented filaments here as discussed above.

F-Actin and Microtubule Distributions After Recovery From CB

The DIC image sequences in Figs. 4 and 5 illustrate that the changes in growth cone structure induced by CB appear to be fully reversible. To assess whether in fact both F-actin and microtubule structures returned to control configurations after exposure to CB, growth cones were treated with CB for 30 min to permit microtubule extension, allowed to recover for 20 min in ASW, and then examined for F-actin and microtubule distributions.

Spatial distributions of F-actin amd microtubules after recovery from CB (Fig. 9 *b*) were similar to those observed

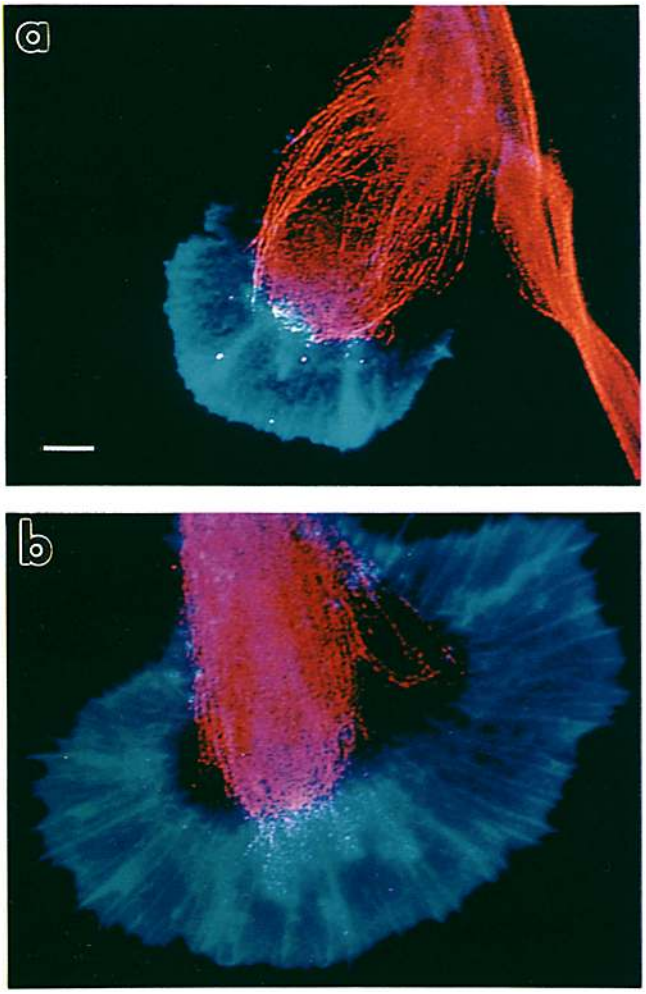

Figure 9. Digital superimposition of F-actin and microtubule spatial domains under control conditions (*a*) and after recovery from a 30-min exposure to CB (*b*). An axonal process runs along right side of field in *a*. SIT camera images of F-actin and microtubule distributions were digitally superimposed to create these composite images. *Red*, microtubules; *blue*, F-actin. Pink areas denote overlap of microtubule and F-actin domains in the transition zone. Bar, 5 μm.

in untreated controls (Fig. 9 *a*) as anticipated from the DIC images. Microtubules receded from the distal growth cone margin showing that CB-induced microtubule extension is a reversible process.

Discussion

Cytochalasins have profound yet entirely reversible effects on growth cone structure and motility (29, 34, 47, 50). In this report, we have examined the effects of cytochalasins on the very large growth cones that terminate *Aplysia* bag cell neurites growing in vitro. Using high resolution digital video microscopy techniques, we have obtained evidence that lamellar motility depends on continuous actin polymerization along the leading edge of the growth cone and also that the actin filament network state may be important in determining microtubule spatial distributions. The effects of CB on actin and microtubule distributions are treated separately below.

An Actin Cycle in Growth Cones

We propose that the waves we observe in time-lapse video result from the retrograde flow of F-actin networks assembled at the distal growth cone margin. This putative actin flow is sustained by ongoing actin polymerization and network assembly at the leading edge of the growth cone and network disassembly and depolymerization in the central transition zone. A local actin cycle is necessary to support such a flow model; the retrograde flow of cortical F-actin networks being balanced by an approximately equal anterograde diffusion or other flux of actin monomers. An actin cycle of this type has recently been proposed as a general concept for understanding cell surface motility and locomotion in animal cells (9).

We interpret the initial effects of CB (i.e., recession of lamellar actin networks) to be the direct result of barbed-end actin filament capping and the resultant inhibition of actin filament elongation along the distal growth cone margin. Filament capping immediately after CB treatment probably causes the abrupt cutoff of actin network assembly that is clearly captured in Figs. 4 *b*; 5 *c*; and 6, *b* and *c*. It is interesting to note that these acutely "capped" actin networks recede steadily at rates comparable to control wave rates (3–8 μm/min) suggesting that actin translocation itself does not depend on distal actin polymerization for motive force.

Other possible explanations for the abrupt loss of distal actin networks we observe after CB treatment might include: cytoplasmic actin network contraction and distal actin network disassembly. Examination of both DIC and rhodamine-phalloidin labeling patterns in acutely treated growth cones (Fig. 6) suggest these alternative explanations are unlikely. Distortion of F-actin labeling patterns would be expected if the distal networks were undergoing contraction (shrinkage). In fact, apart from the obvious recession from the leading edge, lamellar actin patterns after brief CB exposure resemble controls, suggesting that distal actin networks recede as a relatively unperturbed unit mass. There is little evidence of filament disruption along the distal edge of the receding F-actin mass as would be expected if network disassembly or filament severing were taking place here and the radial alignment of actin bundles characteristic of lamellar actin networks under control conditions appears unperturbed (Fig. 6, *c* and *e*). These observations support the hypothesis that the initial effects of CB result primarily from actin filament capping along the distal growth cone margin and not from other disruptive effects. Actin depolymerization mechanisms are unlikely because depolymerization is not among the well-characterized actions of CB (7, 10, 13, 15, 19, 30, 33, 35, 46).

Recovery of normal lamellar motility and actin structure after CB treatments occurred preferentially along the leading growth cone edge where a dense actin matrix formed and subsequently expanded centripetally during the recovery process (Fig. 8). A similar pattern of actin network reconstitution has been observed in fibroblasts recovering from treatment with metabolic inhibitors (43). The pattern of events accompanying recovery of actin polymerization in both growth cones and fibroblasts then suggests that preferential actin polymerization and network assembly occurs along lamellar borders.

What is the origin and significance of the "coarse" isotropic actin matrix we observe forming in proximal regions of the

growth cone during the initial phase of recovery from CB? When CB dissociates from an actin filament during washout, the barbed end can act as a nucleation site or may anneal with another short filament to form a longer one. Many short actin filaments are likely to be present in the aggregates of F-actin randomly distributed throughout the lamellar region after CB treatment (see Fig. 7 *e*; reference 45). The coarse matrix is observed to form with actin aggregates as interfilament foci (Fig. 5, *e* and *f*, *arrows*) which appear to shrink as the coarse matrix forms, suggesting that they may act as actin reservoirs for coarse matrix assembly. Note that the coarse matrix undergoes retrograde translocation until it is replaced by the flow of dense matrix assembled at the leading edge of the growth cone. Retrograde translocation of both coarse and dense actin matrices suggests then that actin filament assembly at the leading edge is not a necessary prerequisite for translocation. Possible mechanisms for actin translocation are considered further below.

The persistent CB-resistant bead of rhodamine–phalloidin labeling along the distal growth cone margin suggests that a population of stable actin oligomers may be localized here (Figs. 6, *c* and *e*; 7 *e*). These oligomers may act as actin nucleation sites for the preferential actin assembly that appears to occur here under control conditions. An analogous situation may exist in both erythrocytes and in brain where F-actin is bound in ternary complexes of actin oligomer, spectrin (fodrin), and band 4.1. These complexes are thought to mediate membrane–actin associations through interaction with membrane protein band 3 (16, see reference 12 for related review).

Previous studies on membrane–cytoskeleton interactions in nonmuscle cells have shown that actin filaments are often oriented with their barbed ends toward membrane attachment sites and also that actin filaments elongate from their membrane-associated ends (37, 38, 44). Assuming for the moment a barbed-end distal actin polarity, F-actin interactions with fixed (stationary relative to the substrate) nonmuscle myosin motors could account for the retrograde actin translocation we observe in growth cones. Two intriguing but as yet unanswered mechanistic questions concern: (*a*) the identity of the putative actin binding mechanochemical motor; and (*b*) its localization. Motor molecule localization is important when considering the forces underlying actin network movement. For example, a "pull" mechanism predicts proximal localization of the mechanochemical motors (probably in the transition zone) to reel in distally generated actin networks; conversely, a homogeneous spatial distribution of motors would be expected if actin networks can either "crawl" or contract as independent volume elements anywhere in the growth cone lamella.

The maximum wave velocity generated by any of the translocation mechanisms suggested above would be limited by the rate of actin polymerization and subsequent network assembly at the leading growth cone edge. Can actin polymerization suport such a process? In a cell-free system, actin polymerization can account for linear polymer growth at ~4 μm/min which is close to the wave rates we see in living cells (assuming a conservative cytoplasmic G-actin concentration of 1 μM [25] and on-rates of 12.3–12.9 molecules/s/μM; reference 8). Thus, a model for lamellar motility that depends on actin polymerization does not appear to conflict with molecular kinetic restraints.

F-Actin and Microtubule Domains

Our results also demonstrate an essentially complementary distribution between F-actin and microtubule domains in motile growth cones; microtubules reside mostly in the central cytoplasmic domain where they support directed organelle transport, whereas F-actin is primarily localized peripherally in lamellae. CB treatment rapidly alters this typical actin/microtubule spatial distribution suggesting that dynamic interactions exist between the contractile microfilament system and microtubules in growth cones. Such interactions between microfilament and microtubule systems have been implicated by previous biochemical studies (42).

What causes microtubule extension in the presence of CB; i.e., in the absence of F-actin networks? Under control conditions, F-actin and microtubule domains in growth cones overlap slightly in the transition zone (Figs. 2 and 9 *a*); however, microtubules are excluded from the dense actin matrix found in lamellae. After prolonged CB treatment actin networks are totally disrupted and microtubules now extend to the distal growth cone edge and often form complicated looped structures in the neurite ending (cf. Fig. 4 *c*). These changes in microtubule distribution after disruption of actin networks by CB raise some basic questions about actin–microtubule interactions. Is microtubule extension due to relief of physical restraints (steric hindrance) normally imposed by peripheral actin networks on microtubules? The functional pore diameter in the intact lamellar actin matrix may exclude microtubules as it appears to exclude larger organelles. In this case the lamellar actin matrix would in essence create a physical barrier to microtubule elongation. It is interesting to note that the gel exclusion diameter characteristic of fibroblast lamellar domains assayed with fluorescently labeled ficols is 25 nm (32). This exclusion limit corresponds well with the diameter of microtubules and clearly supports the physical exclusion hypothesis suggested above. The exclusion/barrier concept is also consistent with the proposal by Joshi et al. (23) that microtubule elongation in growth cones may be regulated by compressive forces generated between microtubules ends and dense peripheral actin networks. Another possibility is that microtubules are normally restrained in the transition zone by associations with actin filaments mediated by microtubule-associated actin-binding protein(s) (cf. reference 42). CB treatment would shunt and inactivate this form of microtubule regulation as well.

A closely related issue is the molecular mechanism of CB-induced microtubule extension. To clearly understand this process it will be necessary to differentiate between microtubule polymerization and microtubule sliding mechanisms (41).

Recent evidence suggests that the growth cone's primary role is to provide growing neurites with a guidance system during development (5), taking molecular cues from the environment in order to lead the neurite to the appropriate target site. After target recognition, the highly motile growth cones are transformed into stable endings capable of stimulus evoked neurosecretion. What cytoskeletal rearrangements are necessary to orchestrate these changes? We have shown here that extension of microtubules occurs spontaneously in growth cones after disruption of actin networks. A distal shift in organelle transport during growth cone–nerve terminal maturation must necessarily occur to accommodate delivery

of secretory granules or synaptic vesicles to a destination near active release sites. Our results show that disruption of actin polymerization and networks in growth cones results in such a shift in organelle transport. Thus, mechanisms by which neurons exert control over growth cone motility may also play an important role in neuronal differentiation.

Received for publication 20 April 1988, and in revised form 17 June 1988.

References

1. Abercrombie, M., J. E. M. Heaysman, and S. M. Pegrum. 1970. The locomotion of fibroblasts in culture. *Exp. Cell Res.* 62:382–398.
2. Allen, R. D., N. S. Allen, and J. L. Travis. 1981. Video-enhanced contrast, differential interference contrast (AVEC-DIC) microscopy: a new method capable of analyzing microtubule-related motility in the reticulopodial network of *Allogromia laticollaris*. *Cell Motil.* 1:291–302.
3. Argiro, V., M. B. Bunge, and M. I. Johnson. 1984. Correlation between growth form and movement and their dependence on neuronal age. *J. Neurosci.* 4:3051–3062.
4. Barak, L. S., R. R. Yocum, E. A. Nothnagal, and W. W. Webb. 1980. Fluorescence staining of the actin cytoskeleton in living cells with 7-nitrobenz-2-oxy-1,3-diazole-phallacidin. *Proc. Natl. Acad. Sci. USA.* 77: 980–984.
5. Bentley, D., and A. Toroion-Raymond. 1986. Disordered pathfinding by pioneer neurone growth cones deprived of filopodia by cytochalasin treatment. *Nature (Lond.).* 323:712–715.
6. Bonder, E. M., and M. S. Mooseker. 1983. Direct electron microscopic visualization of barbed end capping and filament cutting by intestinal microvillar 95-kdalton protein (villin): a new actin assembly assay using the *Limulus* acrosomal process. *J. Cell Biol.* 96:1097–1107.
7. Bonder, E. M., and M. S. Mooseker. 1986. Cytochalasin B slows but does not prevent monomer addition of the barbed end of the actin filament. *J. Cell Biol.* 102:282–288.
8. Bonder, E. M., D. J. Fishkind, and M. S. Mooseker. 1983. Direct measurement of critical concentrations and assembly rate constants at the two ends of an actin filament. *Cell.* 34:491–501.
9. Bray, D., and J. G. White. 1988. Cortical flow in animal cells. *Science (Wash. DC).* 239:833–888.
10. Brown, S. S., and J. A. Spudich. 1981. Mechanism of action of cytochalasin: evidence that it binds to actin filaments. *J. Cell Biol.* 88:487–491.
11. Casella, J. F., D. J. Maack, and S. Lin. 1986. Purification and initial characterization of a protein from skeletal muscle that caps the barbed ends of actin filaments. *J. Biol. Chem.* 261:10915–10921.
12. Chasis, J. A., and S. B. Shohet. 1987. Red cell biochemical anatomy and membrane properties. *Annu. Rev. Physiol.* 49:237–248.
13. Cooper, J. A. 1987. Effects of cytochalasin and phalloidin on actin. *J. Cell Biol.* 105:1473–1478.
14. Dunn, G. A., and J. P. Heath. 1976. A new hypothesis of contact guidance in tissue cells. *Exp. Cell Res.* 101:1–14.
15. Flanagan, M. D., and S. Lin. 1980. Cytochalasins block actin filament elongation by binding to high affinity sites associated with F-actin. *J. Biol. Chem.* 255:835–838.
16. Flanagan, M. D., D. C. Lin, and S. Lin. 1986. Specific association of brain spectrin with actin and erythrocyte band 4.1. *In* Membrane Skeletons and Cytoskeletal–Membrane Associations. V. Bennett, C. M. Cohen, S. E. Lux, and J. Palek, editors. Alan R. Liss, Inc., New York. 243–252.
17. Forscher, P., L. K. Kaczmarek, J. Buchanan, and S. J. Smith. 1987. Cyclic AMP induces changes in distribution of organelles within growth cones of *Aplysia* bag cell neurons. *J. Neurosci.* 7:3600–3611.
18. Goddette, D. W., and C. Frieden. 1986. Actin polymerization. The mechanism of action of cytochalasin D. *J. Biol. Chem.* 261:15974–15980.
19. Hartwig, J. H., and T. P. Stossel. 1979. Cytochalasin B and the structure of actin gels. *J. Mol. Biol.* 134:539–553.
20. Heath, J. P. 1983. Direct evidence for microfilament-mediated capping of surface receptors on crawling fibroblasts. *Nature (Lond.).* 302:532–534.
21. Inoue, S. 1981. Video image processing greatly enhances contrast, quality, and speed in polarization-based microscopy. *J. Cell Biol.* 89:346–356.
22. Isenberg, G., U. Aebi, and T. D. Pollard. 1980. An actin-binding protein from *Acanthamoeba* regulates actin filament polymerization and interactions. *Nature (Lond.).* 288:455–459.
23. Joshi, H. C., D. Chu, R. E. Bauxbaum, and S. R. Heidemann. 1985. Tension and compression in the cytoskeleton of PC 12 neurites. *J. Cell Biol.* 101:697–705.
24. Kater, S., and P. Letourneau. 1985. Biology of the Nerve Growth Cone. Alan R. Liss, Inc., New York. 347 pp.
25. Korn, E. D. 1982. Actin polymerization and its regulation by proteins from nonmuscle cells. *Physiol. Rev.* 62:672–737.
26. Letourneau, P. 1981. Immunological evidence for colocalization in neurite growth cones of actin and myosin and their relationship to cell-substratum adhesions. *Dev. Biol.* 85:113–122.
27. Letourneau, P. C. 1985. Axon growth and guidance. *In* Molecular Basis of Neural Development. G. M. Edelman, W. E. Gall, and W. M. Cowan, editors. John Wiley and Sons, New York. 269–294.
28. Letourneau, P. C., and A. H. Ressler. 1983. Differences in the organization of actin in the growth cones compared with the neurites of cultured neurons from chick embryos. *J. Cell Biol.* 97:963–973.
29. Letourneau, P., T. A. Shattuck, and A. H. Ressler. 1987. "Push" and "Pull" in neurite elongation: observations on the effects of different concentrations of cytochalasin B and taxol. *Cell Motil.* 8:193–207.
30. Lin, D. C., K. D. Tobin, M. Grumet, and S. Lin. 1980. Cytochalasins inhibit nuclei-induced actin polymerization by blocking filament elongation. *J. Cell. Biol.* 84:455–460.
31. Lin, S., and J. A. Spudich. 1974. Biochemical studies on the mode of action of cytochalasin B. Cytochalasin B binding to red blood cell membrane in relation to glucose transport. *J. Biol. Chem.* 249:5778–5783.
32. Luby-Phelps, K., and D. L. Taylor. 1988. Subcellular compartmentalization by local differentiation of cytoplasmic structure. *Cell Motil. Cytoskeleton.* 10:28–37.
33. MacLean-Fletcher, S., and T. D. Pollard. 1980. Mechanism of action of cytochalasin B on actin. *Cell.* 20:329–341.
34. Marsh, L., and P. C. Letourneau. 1986. Growth of neurites without filopodial or lamellar activity in the presence of cytochalasin B. *J. Cell Biol.* 2041–2047.
35. Maruyama, K., J. H. Hartwig, and T. P. Stossel. 1980. Cytochalasin B and the structure of actin gels II: further evidence for the splitting of F-actin by cytochalasin B. *Biochim. Biophys. Acta.* 626:494–500.
36. Miranda, A. F., G. C. Godman, A. D. Deitch, and S. W. Tanenbaum. 1974. Action of cytochalasin D on cells of established lines. *J. Cell Biol.* 61:481–500.
37. Mooseker, M. S., and L. G. Tilney. 1975. The organization of an actin filament–membrane complex: filament polarity and membrane attachment in the microvilli of intestinal epithelial cells. *J. Cell Biol.* 67:725–743.
38. Mooseker, M. S., T. D. Pollard, and K. A. Wharton. 1982. Nucleated polymerization of actin from the membrane-associated ends of microvillar filaments in the intestinal brush border. *J. Cell Biol.* 95:223–233.
39. Oster, G. 1984. On the crawling of cells. *J. Embryol. Exp. Morphol.* 83:329–364.
40. Pollard, T. D. 1986. Actin and actin-binding proteins. A critical evaluation of mechanisms and functions. *Annu. Rev. Biochem.* 55:987–1035.
41. Schulze, E., and M. Kirschner. 1987. Dynamic and stable populations of microtubules in cells. *J. Cell Biol.* 104:277–288.
42. Selden, S. C., and T. D. Pollard. 1983. Phosphorylation of microtubule-associated proteins regulate their interaction with actin filaments. *J. Biol. Chem.* 258:7064–7071.
43. Tatjana, M. S., A. A. Neyfakh, and A. Bershadsky. 1986. Actin cytoskeleton of spread fibroblasts appears to assemble at the cell edges. *J. Cell Sci.* 82:235–248.
44. Tilney, L. G., E. M. Bonder, and D. J. DeRosier. 1981. Actin filaments elongate from their membrane-associated ends. *J. Cell Biol.* 90:485–494.
45. Weber, K., P. C. Rathke, M. Osborne, and W. W. Franke. 1976. Distribution of actin and tubulin in cells and in glycerinated cell models after treatment with cytochalasin B (CB). *Exp. Cell Res.* 102:285–297.
46. Weihing, R. R. 1976. Cytochalasin B inhibits actin-related gelation of HeLa cell extracts. *J. Cell Biol.* 71:303–307.
47. Wessells, N. K., B. S. Spooner, J. F. Ash, M. O. Bradley, M. A. Luduena, E. L., Taylor, J. T. Wrenn, and K. M. Yamada. 1971. Microfilaments in cellular and developmental processes. *Science (Wash. DC).* 171: 135–143.
48. Wieland, T., J. X. De Vries, A. Schafer, and H. Faulstich. 1975. Spectroscopic evidence for the interaction of phalloidin with actin. *FEBS (Fed. Eur. Biochem. Soc.) Lett.* 54:73–75.
49. Wulf, E., F. A. Bautz, H. Faulstich, and T. Wieland. 1979. Fluorescent phallotoxin, a tool for the visualization of cellular actin. *Proc. Natl. Acad. Sci. USA.* 76:4498–4502.
50. Yamada, K. M., B. S. Spooner, and N. K. Wessells. 1971. Ultrastructure and function of growth cones and axons of cultured nerve cells. *J. Cell Biol.* 49:614–635.